Reacting Shock Layers with Slip and Catalytic Boundary Conditions

Carl D. Scott*
NASA Johnson Space Center, Houston, Tex.

The influence of wall slip and catalytic atom-recombination on the flowfield and wall heat flux are calculated for high-altitude flight and arcjet-flow conditions. Boundary equations, which include velocity slip, temperature jump, and wall catalytic atom-recombination, are coupled to the viscous reacting multicomponent Navier-Stokes equation. These equations are solved using a time-dependent finite difference technique applied to spheres in an arcjet flow (Reynolds number of 550) and a high-altitude flight case representative of the space shuttle orbiter (Reynolds number of 450). The results indicate that catalysis strongly influences the temperature jump, but not the velocity slip. Slip increases the atom fraction and temperature at both the wall and in the flowfield. Likewise, the shock stand-off distance, the wall heat flux, and friction coefficient are increased over the nonslip cases. The reacting gas calculations confirm the chemically frozen nature of the shock layer in arcjet flows.

I. Introduction

TO design the reusable space shuttle orbiter for high-altitude, low Reynolds number, atmospheric entry necessitates a more comprehensive treatment and understanding of the interaction between a high enthalpy gas flow and a relatively cold surface. At low densities the continuum model of the gas breaks down in regions of large gradients such as those near a cold body. Corrections to the equations for the boundary conditions are then required for the flow. These influences are reflected in the calculations of surface heat-transfer rate and chemical composition of the flow near the wall. The aim of this paper is to quantify how these low density phenomena interact, how they influence interpretation of test data obtained on thermal protection systems, and how they alter the predictions of heating rates and performance of the space shuttle orbiter thermal protection system (TPS) during its long high-altitude entry.

The approach taken here is to obtain finite difference solutions to the reacting Navier-Stokes equations for the flow around spheres in both space shuttle flight and arcjet environments. The wall boundary conditions for these solutions are obtained from slip and jump relations for a nonequilibrium multicomponent gas mixture. They include the effects of catalytic atom recombination. From the solutions one can assess the effects of the boundary conditions on the flow properties, the heat flux, etc.

At low densities, the continuum-flow equations are no longer adequate close to the wall because the mean free path becomes long compared to characteristic lengths associated with significant changes in macroscopic-flow parameters. The flow in a region next to the wall having a thickness on the order of a mean free path (the Knudsen layer) cannot be described by the Navier-Stokes description (Kogan[1]). To determine the flow properties within the Knudsen layer requires the direct solution of the Boltzmann equation matched to the solutions for the outer flow (Navier-Stokes equation) and the wall boundary condition. This is most conveniently done through the use of a slip model in which slip and jump properties are used for the boundary conditions for the Navier-Stokes equations.

Presented as Paper 74-174 at the AIAA 12th Aerospace Sciences Meeting, Washington, D.C., January 30-February 1, 1974; submitted March 1, 1974; revision received March 27, 1975.

Index categories: Viscous Nonboundary-Layer Flows; Reactive Flows; Supersonic and Hypersonic Flows.

*Research Scientist, Thermal Technology Branch.

The slip and jump equations used in the present calculation are of the type originally proposed by Maxwell[2] and modified to account for a more exact distribution function (see, for example, Patterson[3] and Shidlovskiy.[4] Scott[5] applied the method to multicomponent mixtures using Chapman-Enskog distribution functions. This method is approximate because instead of solving the Boltzmann equation it neglects changes in the distribution function across the Knudsen layer. This assumption leads to errors in the jump conditions of typically less than 15%.[6]

Figure 1 is a stagnation pressure vs total enthalpy plot showing typical entry trajectories for the space shuttle orbiter and the Apollo command module. It also shows regions where arc heated wind tunnels typically operate for entry environment simulation. The approximate region in which slip effects become important is indicated in this figure. It can be seen that there is a portion of the shuttle trajectory where slip may have a significant effect on the boundary conditions. Moreover, slip is significant for a large portion of the illustrated typical arc tunnel simulation region. It is evident

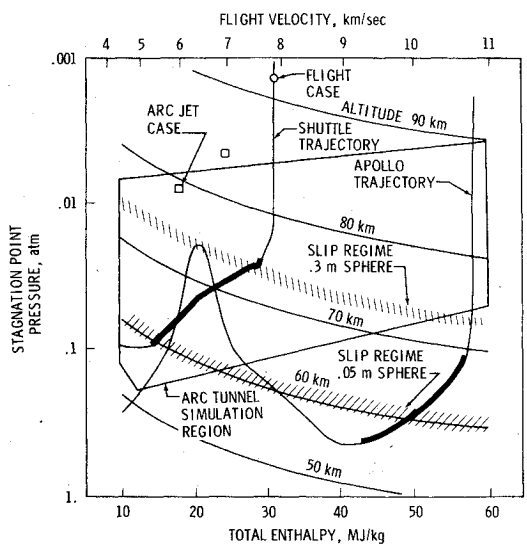

Fig. 1 Stagnation pressure vs enthalpy plot showing shuttle and Apollo trajectories with typical arc jet operating map. The region of peak heating rates for the Shuttle and Apollo are indicated by the thick portion of the trajectory curves.

Table 1 Flowfield freestream properties

	Arcjet	Flight
Knudsen number	0.022	0.10
Mach number	8.0	30.7
Reynolds number	553.	450.
Altitude, km	...	91.5
Velocity, km/sec	4.12	7.93
Total enthalpy, MJ/kg	17.6	31.5
Temperature, K	414.	164.
Pressure, N/m^2	11.28	0.101
Density, kg/m^3	6.41×10^{-5}	2.13×10^{-5}
Wall temperature, K	400.	1640.
Radius of sphere, cm	5.08	30.5
Species mass fractions		
N_2	0.6124	0.767
O_2	0.1084×10^{-4}	0.233
N	0.1522	...
O	0.2347	...
NO	0.3761×10^{-4}	...
NO^+	0.6849×10^{-5}	...
e^-	0.1187×10^{-9}	...

that the greatest significance of slip and catalytic phenomena to the space shuttle orbiter TPS development is in the interpretation of arc jet test data.

In the past, shock layer[7-11] and flowfield[12] calculations have been made which incorporate various gas models and limited combinations of the boundary conditions under consideration. In this paper, boundary equations for slip and catalytic wall recombination have been coupled to a two-dimensional viscous reacting blunt body flowfield solution developed by Li.[12] The computations are made using a time-dependent finite difference technique which includes a seven-species air model. Results are presented for spheres at both a typical moderate enthalpy arcjet flow and a flight condition (Fig. 1). The freestream properties for the arcjet condition, which are calculated using a one-dimensional inviscid-reacting gas nozzle flow computer program,[13] are given in Table 1.

Calculations are presented for a range of boundary conditions in both the arcjet and flight cases. The boundary conditions at the wall include: 1) fully catalytic, 2) noncatalytic, and 3) finite recombination coefficients (see Table 2). An isothermal wall boundary condition and full accommodation are used in all cases.

II. Analysis and Numerical Technique

A. Boundary Conditions

The wall boundary equations[5] used in the calculations were developed for a mixture of gases where the species, momenta, and energy fluxes are matched across the Knudsen layer, which is a layer on the order of one mean free path next to the wall. The jump in properties at the wall is treated as discontinuous across an arbitrarily thin Knudsen layer, and no account is taken of variations in the velocity distribution functions through the Knudsen layer. The distribution functions at the wall are described to first-order accuracy (Navier-Stokes approximation) by a Chapman-Enskog expansion for a nonuniform multicomponent mixture obtained through the variational method of Hirschfelder, Curtiss, and Bird.[14] The molecules which specularly reflect from the wall are characterized by the temperature of the gas (slip temperature). Those diffusely reflected are characterized by the wall temperature. The balance equations for momentum and energy flux are summed over species and coupled with the species flux balance equations to obtain the slip velocity and temperature jump.†

†Slip boundary equations obtained via the Boltzmann equation were recently published by Cipolla, Lang, and Loyalka.[15] These should be more accurate than the ones used in the present work. However, they were not available to the author at the time of the flowfield calculations, nor do they include velocity slip.

1) Gas/wall interaction

Gas molecules striking the wall are assumed either to stick and become fully accommodated or reflect specularly without any accommodation. A single accommodation coefficient for species "i" θ_i is defined as the fraction of those molecules which strike the surface, stick, and subsequently leave the surface at the wall temperature. The change in internal energy of the reflecting molecules such as vibrational and electronic excitation is neglected. In these calculations θ_i is set equal to unity for all species because detailed measurements of the accommodation coefficients have not been made. Atoms which strike the surface may stick and recombine to form molecules. The fraction striking the surface that recombines is defined as the recombination coefficient γ_i.

2) Balance equations

To obtain the slip boundary equations for the gas/solid interface, the net fluxes of species, momentum, and energy at the outer edge of the Knudsen layer are equated to the difference between the incident and reflected fluxes at the wall. It is assumed that these fluxes are constant across the Knudsen layer. The fluxes are obtained from moments of the distribution function. For example, if $\phi(V)$ is a molecular property such as mass, momentum, or energy, then the net flux of that property normal to the wall at the outer edge of the Knudsen layer is

$$F=\int_{-\infty}^{\infty}\int_{-\infty}^{\infty}\int_{-\infty}^{\infty} V_y\phi(V)f_s(V)d^3V \tag{1}$$

where V_y is the normal component of the molecular velocity and $f_s(V)$ is the velocity distribution function at the edge of the Knudsen layer (see Fig. 2).

Analogous integrals for the incident and reflected fluxes are obtained by integrations over appropriate half-spaces in molecular velocity. The diffusely reflected fluxes are obtained using the wall velocity distribution function $f_w(V)$. Thus

$$F^i=\int_{-\infty}^{\infty}\int_{-\infty}^{0}\int_{-\infty}^{\infty} V_y\phi(V)f_s(V)d^3v \tag{2}$$

is the incident flux.

$$F^r=\int_{-\infty}^{\infty}\int_{0}^{\infty}\int_{-\infty}^{\infty} V_y\phi(V)f_s(V_x,-V_y,V_z)d^3V \tag{3}$$

is the specularly reflected flux.

$$F_w=\int_{-\infty}^{\infty}\int_{0}^{\infty}\int_{-\infty}^{\infty} V_y\phi(V)f_w(V)d^3v \tag{4}$$

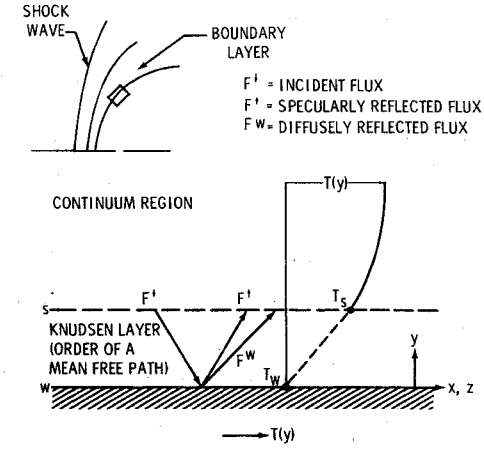

Fig. 2 The Knudsen layer showing general fluxes and coordinate axes. The temperature as a function of normal distance is schematically overlayed.

is the diffusely reflected flux.

The general flux balance equation therefore is

$$\sum_i F_i = \sum_i F_i^{\dagger} + \sum_i (1-\theta_i) F_i^{\dagger} + \sum_i (\theta_i - \gamma_i) F_{w_i} \qquad (5)$$

where the sum is over species. The sum is deleted for a species balance equation.

3) Slip equations

By substituting Eqs. (2-4) into Eq. (5) and carrying out the integrations for species, momentum, and energy, one obtains equations relating the slip properties to wall properties and gradients at the edge of the Knudsen layer.

$$v_{0_x}^s = \frac{1}{\sum_i \left[\frac{m_i}{2kT_s}\right]^{1/2} p_i^s} \left\{ \sqrt{\pi}\, \frac{2-\theta}{2\theta}\, \eta \left[\frac{\partial v_{0_x}}{\partial y} + \frac{\partial v_{0_y}}{\partial x} \right]_s + \sum_i \frac{p_i^s}{2} \left[-a_{il} \frac{\partial \ln T}{\partial x} - n \sum_j c_{i_0}^{(j)} d_{j_x} \right] \right\}_s \qquad (6)$$

$$T_s = \frac{1}{2k} \left\{ \frac{2\sqrt{\pi}\left[\frac{2-\theta}{2\theta}\right] E_y - (2k)^{3/2} T_w \sum_i \left\{ \frac{1}{\sqrt{m_i}} \frac{n_i^s}{2} T_s^{1/2} \left[1 + \frac{P_{iy}}{P_i^s} \right] + \sqrt{\pi}\, \frac{2-\theta_i}{\theta_i} (1/2k)^{1/2} \frac{M_{iy}}{m_i} \right\}}{- \sum_i \frac{n_i^s}{\sqrt{m_i}} - \frac{3}{4KT_s} \sum_i \frac{1}{\sqrt{m_i}} \tau_{yy_i}} \right\}^{2/3} \qquad (7)$$

$$n_i^s = \frac{-((2-\gamma_i)/2\gamma_i)(2\pi m_i/kT_s)^{1/2} (M_{iy}/m_i)}{\frac{1}{2}(1 + (P_{iy}/p_i))_s} \qquad (8)$$

(for recombining species)

In these equations η is the viscosity; E_y is the normal heat flux due to conduction; M_{iy} is the normal mass flux of species "i"; P_{iy} is the normal momentum flux; τ_{yy_i} is the normal shear stress; τ_{xy_i} is the tangential shear stress; and p_i is the partial pressure of species "i." All these are evaluated at the edge of the Knudsen layers. The wall termperature is T_w. The Appendix contains explicit expressions for the net fluxes. The constants a_{il}, b_{i0}, $c_{i0}^{(j)}$, determined from the Curtiss and Hirschfelder[16] variation problem in the first approximation for a mixture, are functions of the collision integrals and are related to the transport properties. The explicit forms of the constants are given in Appendix A of Ref. 5. The vector $\boldsymbol{d}_j$ is related to the diffusion velocity of the j^{th} species in the mixture and is approximately equal to the concentration gradient.

$$\boldsymbol{d}_j = \nabla (n_j/n) \qquad (9)$$

where n_j is the number density of the j^{th} species and n is the total number density. Pressure diffusion and thermal diffusion are neglected because these are second-order effects. The total mass-averaged velocity is $\boldsymbol{v}_0$.

To use simplified transport coefficients and thus not have to calculate the parameters a_{il}, b_{i0}, and $c_{i0}^{(j)}$ for all species, the slip equations were simplified by assuming the τ_{yy_i}, τ_{yy_i}, E_{i_x}, and P_{i_y} are the same for all species and equal to the corresponding total fluxes. This approximation retains the major effects of multicomponent fluxes on the slip velocity and temperature jump.

These equations reduce exactly to the form given by Patterson[3] for a simple gas and unit accommodation coefficients. Patterson's equations agree with corresponding equations obtained by a more exact method—an approximate Boltzmann equation solution Ref. 1, p. 382)—to within about 15% for the conditions studied in this paper.

B. Flowfield Equations

The flowfield equations used in the calculations are the fully viscous reacting Navier-Stokes equations in conservative form. Details of the transformations used to convert these equations to the computational coordinate system and explicit expressions for the various terms in the equations are given in Ref. 12.

The coordinate system used in the calculations is a body-intrinsic frame, as shown in Fig. 3. The independent variables are surface distance S, normal distance y, and time t. The computational domain is bounded by the upstream boundary $y = Y(S)$ for which all properties are assigned freestream values, e.g., $T_\infty, v_\infty, p_\infty, e_\infty$, and ρ_∞. Thus, the shock wave develops within the computational domain (see discussion in Ref. 17). The boundary conditions at the downstream boundary $S = S_{\max}$ are obtained by linearly extrapolating the dependent variables for the flow equations from interior points to the downstream boundary. The boundary conditions on the wall for the slip-flow cases have been given in Sec. II A,3).

For the nonslip cases, the wall boundary conditions are

$$u = v = 0$$

$$T = T_w$$

The species mass fraction boundary conditions are

$$c_\ell = c_\ell(T_w)$$

for a catalytic wall and

$$\partial c_\ell / \partial y = 0$$

for a noncatalytic wall. The wall is assumed to be noncatalytic for $NO^+ - e^-$ recombination in the slip cases.

To obtain the wall heat flux and skin friction coefficient, the following expressions are used

$$q_y = -\lambda \frac{\partial T}{\partial y} + \sum_\ell M_{\ell_y} h_\ell \qquad (10)$$

$$C_F = \tau_{ys} / \tfrac{1}{2} \gamma_\infty M_\infty^2 \qquad (11)$$

where λ is the thermal conductivity, h_ℓ is the specific enthalpy of formation of the ℓth species, γ_∞ and M_∞ are the freestream

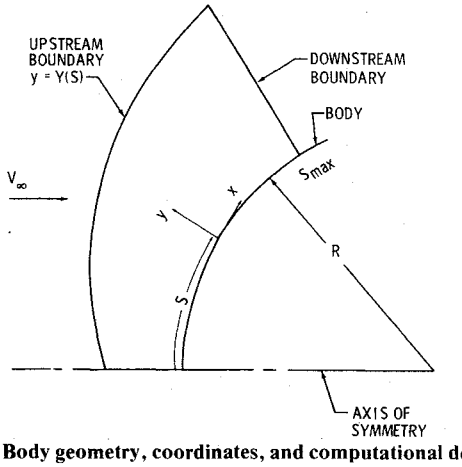

Fig. 3 Body geometry, coordinates, and computational domain.

ratio of specific heats and Mach number, respectively, and τ_{ys} is the shear stress at the wall.

The transport properties are obtained from constant Lewis numbers Le_{ij}, Prandtl number Pr, and Sutherland viscosity η

$$\eta = (3/2)(T/T_\infty)^{3/2}/(T/T_\infty + 1/2) \tag{12}$$

The thermodynamic functions are computed from curve fits of data calculated by a technique given by Svehla[18] and Mc Bride and Gordon.[19] The reaction rates for the seven species gas model were obtained from Vincenti and Kurger.[20]

C. Numerical Technique

The numerical technique as used by Li[12,17] is a second-order difference predictor corrector scheme originally proposed by MacCormack.[21] The Navier-Stokes equations are transformed to finite difference equations and then relaxed in time (a hyperbolic coordinate).

The step size Δt is computed locally at each mesh point. Therefore, for a given time-step all points do not lie on an isochrone. Since this is a relaxation technique such local differences in time do not affect the final solution. The relaxation technique also permits a solution to converge from any reasonable initial conditions.

The computational domain normal to the body is divided into 20 mesh points in the flight cases and 30 mesh points in the arcjet cases. The body is spherical and the outer computational boundary is described as follows

$$Y(S)/R = 0.35 + 0.0015(S/R)^2 \tag{13}$$

for the arcjet cases,

$$Y(S)/R = 0.3 \tag{14}$$

for the flight cases.

III. Results and Discussion

Numerical computations have been performed for two flow conditions. One is a typical arcjet flow in which the freestream air is highly dissociated. The other is a high-altitude entry trajectory point for the space shuttle orbiter. The latter case was selected to assure that the slip phenomena are significant enough to validate the computational procedure. The freestream properties for both cases are presented in Table 1.

Calculations for the two cases are made with various wall boundary conditions of slip and nonslip and various wall catalycities, as summarized in Table 2. In all cases, the assigned recombination coefficients apply to the following reactions

$$N + N \xrightarrow{\gamma} N_2$$

$$O + O \xrightarrow{\gamma} O_2$$

$$NO + NO \xrightarrow{\gamma} O_2 + N_2$$

In the nonslip cases a fully catalytic condition is imposed by assigning zero mass fractions to N,O, and NO at the wall. In all noncatalytic cases ($\gamma = 0$) the boundary condition $c_\ell^n = c_\ell^{n-1}$ is imposed for $\ell = N,O$, and NO (where the supercript n refers to the computational mesh point at the wall and $n-1$ refers to the computational mesh point one step away from the wall.

The calculations were made on a UNIVAC 1108 computer at the Johnson Space Center. A solution was considered to have converged when none of the flow variables changed more than about 2% in 100 time-steps. This cutoff was required to avoid excessively long computation times.

Table 2 Recombination coefficients used in calculations[a]

	Arcjet	Flight
Slip	0, 0.02, 0.2, 1.0	0, 1.0
Nonslip	0, 1.0	0, 1.0

[a] Recombination coefficients for N, 0, and NO were assumed to be equal.

A. Frozen Composition

The flow around the sphere in the arcjet cases was found to be highly frozen with respect to chemical reactions. All mass fractions of the major species are virtually unchanged along the stagnation line.

This is a significant result for more approximate arcjet-flow calculation techniques and analyses. For example, boundary-layer calculations which assume that the edge of the boundary layer is in chemical equilibrium can lead to significant errors in cases where the wall is noncatalytic. The atom fractions at the edge of the boundary layer, particularly nitrogen, will be in error. Hence, the edge temperature would be underpredicted, as well as the heat flux to the wall. In boundary-layer calculations it would be preferable to assume that the composition is frozen at freestream concentrations and that the shock-layer flow behaves as an ideal gas.

B. Temperature Jump

It can be seen in Figs. 4 and 5 that the increase in the atom flux to the wall due to catalytic recombination increases the temperature jump. In the arcjet case, the jump T_s/T_w is on the order of two and slowly increases around the body. In the flight case, the jump is larger an increases more steeply around the body. The jump is larger for a more highly catalytic surface.

The differences in temperature jump for various recombination coefficients are not due to the mass flux terms in the temperature jump equation [Eq. (6)]. Instead, a variation in the molecular weight along the wall leads to the variation in temperature jump.

C. Velocity Slip

The velocity slip is plotted as a function of surface distance around the sphere for the arcjet case in Fig. 6 and the flight case in Fig. 7. These curves are qualitatively similar and exhibit virtually no dependence on wall catalysis, as would be expected, since normal mass fluxes do not enter the velocity boundary equation [Eq. (6)]. The steep rise in slip velocity is due to the increase in shear stress and the increased rarefaction around the body. The absolute magnitude of the slip velocity is small compared to the velocity at the next mesh point away from the wall (order of magnitude smaller); therefore, at the conditions studied here, velocity slip has a negligible effect on the velocities in the flowfield.

D. Species Concentration Jump

Figure 8 shows the distribution of oxygen and nitrogen atom concentrations along the stagnation line with and without slip for a catalytic body. These data were calculated for the flight case discussed herein. It can be seen that the concentrations are not zero at the edge of Knudsen layer ($y/R = 0$) in the slip case. This jump is reflected in higher concentrations in the shock layer and beyond with the peak occurring farther from the body. Part of this increase in atom concentrations is also due to increased temperatures in the shock layer, as seen in Fig. 9. There the normal temperature distributions are plotted along the stagnation line and normal to the body at $S/R = 0.8$. It is seen (the slip curves are displaced with respect to the nonslip curves) that the influence

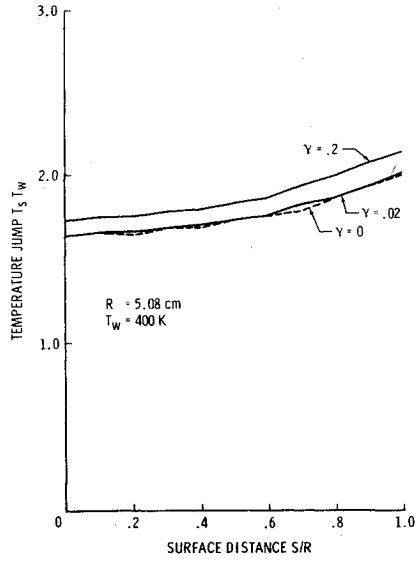

Fig. 4 Temperature jump along isothermal wall in arcjet for various recombination coefficients and unity accommodation coefficients for all species.

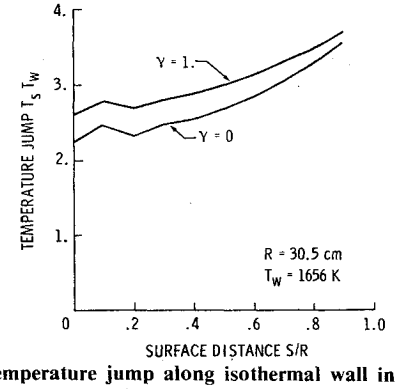

Fig. 5 Temperature jump along isothermal wall in flight case for catalytic and noncatalytic wall. The accommodation coefficients are unity for all species.

of the temperature jump extends out into the shock wave and the peak in temperature occurs farther away from the body than in the nonslip case.

E. Shock Wave and Shock Layer

In these low Reynolds number cases the thick shock wave comprises as much as half the shock layer in the flight case (see Figs. 8, 9, and 10) and approximately 20% of the shock layer in the arcjet case (see Fig. 11). The shock wave is the region of rapid change in temperature and pressure upstream of their peaks. The computational mesh was fine enough in the direction normal to the body to permit the shock wave structure to develop in the calculations. As seen in Figs. 8 and 9, the shock waves stands off farther from the body in the slip cases. This effect increases with distance around the body. In the first case the flow is in the merged viscous flow regime, whereas the flow in the arcjet case has a distinct inviscid region represented by the plateau in T between the shock wave and the boundary layer.

F. Heat Fluxes at Wall

The heat flux at the wall results from conduction and energy transported along with the species mass flux in the form of energy of recombination. The calculations assume that all this energy transported to the wall is absorbed by the wall and that the molecules resulting from recombination of

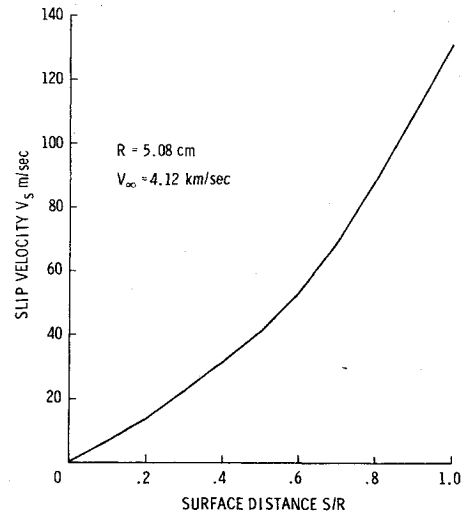

Fig. 6 Slip velocity around isothermal sphere having catalytic recombination coefficients γ of 0, 0.02, 0.2, and 1. The accommodation coefficients are unity for all species, arcjet cases.

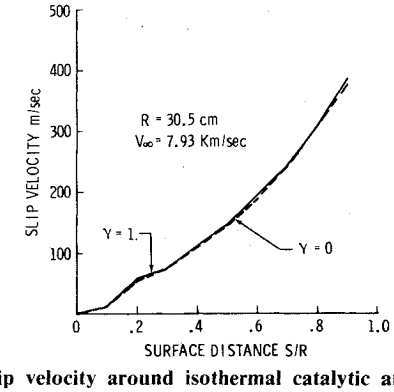

Fig. 7 Slip velocity around isothermal catalytic and noncatalytic walls. The accommodation coefficient is unity for all species, flight cases.

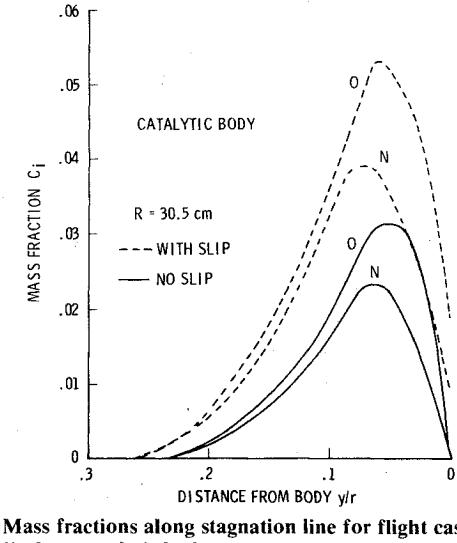

Fig. 8 Mass fractions along stagnation line for flight cases with and wihout slip for a catalytic body.

atoms leave the surface in equilibrium with the wall temperature, that is, they are not in highly excited states. This assumption is commonly made, but this is not strictly true for oxygen recombination on many materials (see Melin and Madix[22]. In rarefield flows this may lead to errors in the heat flux (Rosner and Feng[23]). This effect has not been considered in these calculations.

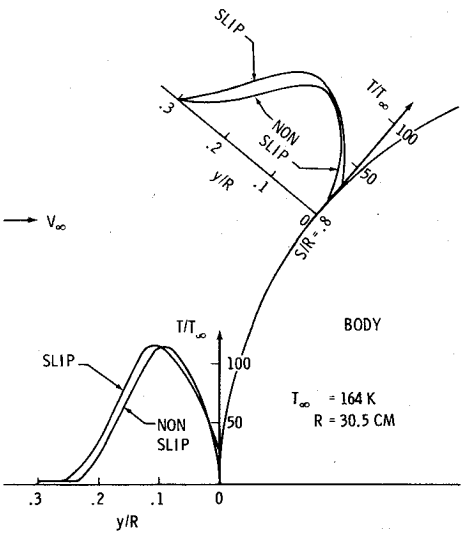

Fig. 9 Temperature distribution normal to body at stagnation line and $S/R = 0.8$ calculated with and without slip boundary conditions for a catalytic wall, flight case.

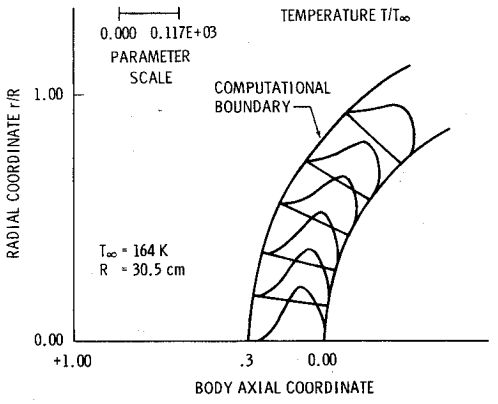

Fig. 10 Temperature distributions normal to wall at various stations around the body for noncatalytic flight case with slip.

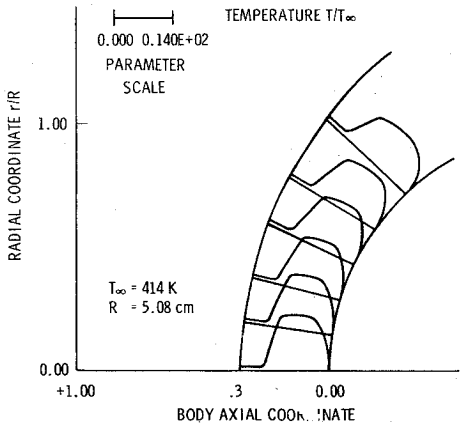

Fig. 11 Temperature distributions normal to wall at various stations around the body for noncatalytic arcjet case with slip.

The heat flux to an isothermal wall for various recombination coefficients are presented in Fig. 12 for the arcjet case. By comparing the slip and nonslip data for a noncatalytic ($\gamma = 0$) surface and similarly for a catalytic ($\gamma = 1$) surface, it is seen that slip increases the heating by 25-30% over the nonslip cases. There is a similar effect in the flight cases (see Fig. 13) but the difference between slip and nonslip

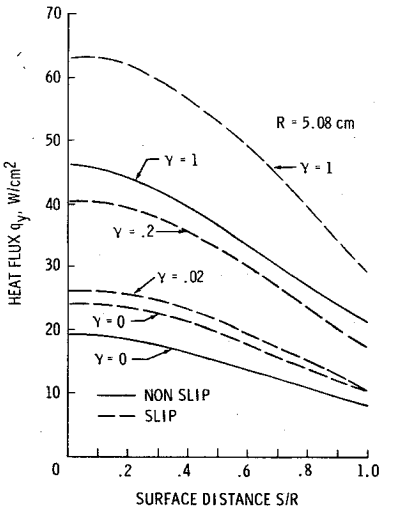

Fig. 12 Heat flux to isothermal wall for various catalytic recombination coefficients with and without slip in arcjet case.

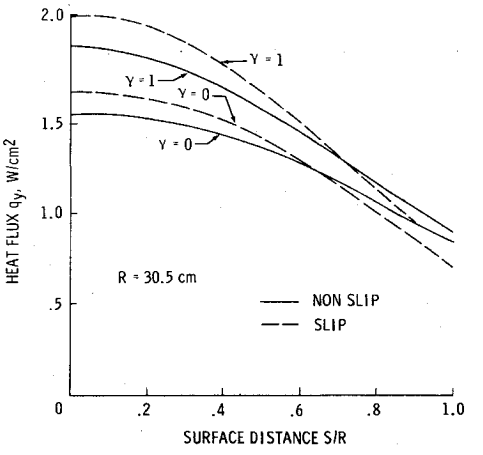

Fig. 13 Heat flux along isothermal wall for catalytic and noncatalytic walls with and without slip for flight case.

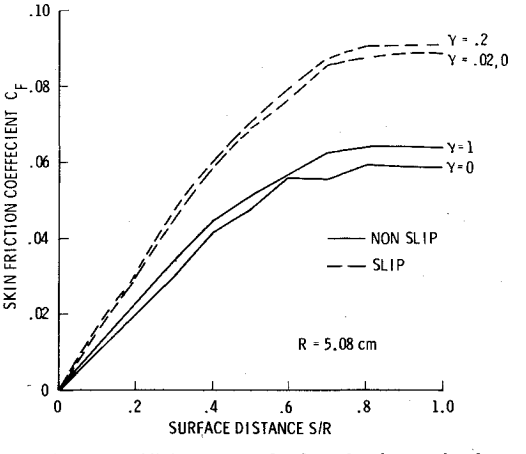

Fig. 14 Friction coefficient around sphere having an isothermal wall for various atom recombination coefficients with and without slip in arcjet flow case.

is not as large (about 10%) in the stagnation region. Around the body the difference goes to zero and in fact the nonslip heat flux becomes larger than the slip. This is due to smaller temperature gradients at larger S/R where the temperature jump is large. In the stagnation region in the flight case the increase in thermal conductivity with temperature appears to dominate the smaller temperature gradient to yield a net increase in the heating rate.

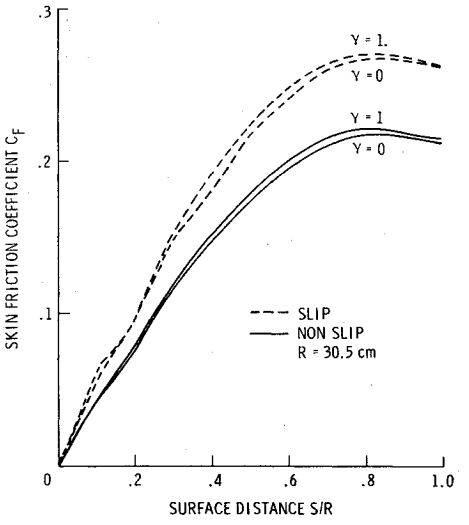

Fig. 15 Friction coefficient around sphere having isothermal wall with and without slip for noncatalytic and catalytic surfaces flight case.

The differences in the contours of the heat-flux distributions with and without slip are readily seen by comparing the heat fluxes for the arcjet and flight cases. One should, therefore, be cautious when extrapolating ground test heating rate distributions to flight, even though the geometries and pressure distributions are similar.

G. Skin Friction

The calculated skin friction coefficients around the spheres are shown in Figs. 14 and 15 for arcjet and flight cases, respectively. The skin friction is larger in the slip-flow cases by 20-30% than in the nonslip cases. This results from an increase in momentum transport due to a higher temperature at the edge of the Knudsen layer rather than velocity slip effects. The effect of catalysis on the skin friction is very small. Differences seen in the plots are probably of numerical accuracy rather than of physical origin. Indeed, the fully catalytic arcjet solution without slip has not reached convergence; therefore, it is subject to larger errors.

IV. Conclusions

A time-dependent finite difference blunt-body flowfield computer program has been used to calculate the effects of wall slip on the flowfield and wall boundary conditions about spheres in the low Reynolds number flows of an arcjet and high-altitude flight. These calculations have shown that including slip boundary conditions increases the heat transfer 20-30% in the arcjet case and less than 10% in the high-altitude flight case. This difference in heating rates would be even less in the maximum heating portion of the space shuttle trajectory.

The effect of slip extends throughout the shock layer by increasing the overall temperature, atom concentrations, and shock standoff distance. These effects are more pronounced in the flight cases where the Knudsen number is higher. The temperature jump increases with catalytic recombination coefficient, whereas the velocity slip is unchanged.

The heat transfer to a noncatalytic wall relative to a catalytic wall is 0.8 in the flight case as compared to 0.4 in the arcjet case. This indicates a need for caution in applying arcjet measured TPS performance characteristics directly to flight. The reacting gas calculations show that the arcjet flow around a sphere is essentially frozen to the freestream conditions; therefore, frozen flow assumptions should be used in simplified calculations.

Appendix

The explicit expressions for the fluxes of mass, momentum, and energy for the ith species are:

$$M_i = \frac{m_i n_i^s n}{2}\left[\frac{2kT_s}{m_i}\right]^{1/2}\sum_j c_{i0}^{(j)} d_j \tag{A1}$$

$$P_{i_y} = p_i^s + \tau_{yy_i} = p_i^s\left[1 + \frac{b_{i0}}{3}\times\left[\frac{\partial v_{0x}}{\partial x} + \frac{\partial v_{0z}}{\partial z} - 2\frac{\partial v_{0y}}{\partial y}\right]\right] \tag{A2}$$

$$\tau_{xy_i} = -p_i^s(b_{i0}/2)\left[(\partial v_{0x}/\partial y) + (\partial v_{0y}/\partial x)\right]_s \tag{A3}$$

$$E_i = \frac{5}{8} m_i n_i^s\left[\frac{2kT_s}{m_i}\right]^{3/2}\left[a_{il}\nabla \ln T + n\sum_j c_{i0}^{(j)} d_j\right]_s \tag{A4}$$

References

[1] Kogan, M. N., *Rarefied Gas Dynamics*, Plenum, New York, 1969, pp. 367-400.

[2] Maxwell, J. C., *Philosophical Transactions of the Royal Society*, I Appendix 1879; reprinted in *The Scientific Papers of J. C. Maxwell*, Dover, New York, 1965.

[3] Patterson, G. N., *Molecular Flow of Gases*, Wiley, New York, 1965, pp. 119-125.

[4] Shidlovskiy, V. P., *Introduction to the Dynamics of Rarefield Gases*, American Elsevier, New York, 1967, pp. 60-68.

[5] Scott, C. D., "Wall Boundary Equations with Slip and Catalysis for Multicomponent Nonequilibrium Gas Flow," NASA TMX 58111, Dec. 1973.

[6] Cercignani, C., *Mathematical Methods in Kinetic Theory*, Plenum, New York, 1969, p. 166.

[7] Davis, R. T., "Hypersonic Flow of a Chemically Reacting Binary Mixture Past a Blunt Body," AIAA Paper 70-805, Los Angeles, Calif., 1970.

[8] Davis, R. T., "Numerical Solution of the Hypersonic Viscious Shock Layer Equations," *AIAA Journal*, Vol. 8, May 1970, pp. 843-851.

[9] Inger, G. R., "Nonequilibrium Hypersonic Stagnation Flow with Arbitrary Surface Catalycity including Low Reynolds Number Effects," *International Journal of Heat Mass Transfer*, Vol. 9, 1966, pp. 759-772.

[10] Blottner, F. G., "Viscous Shock Layer at the Stagnation Point with Nonequilibrium Air Chemistry," *AIAA Journal*, Vol. 7, 1969, pp. 2281-2288.

[11] Jain, A. C. and Adimurthy, V., "Hypersonic Merged Stagnation Shock Layers, Part I: Adiabatic Wall Case," *AIAA Journal*, Vol. 12, March 1974, pp. 342-347, "Part II: Cold Wall Case," *AIAA Journal*, Vol. 12, March 1974, pp. 348-354.

[12] Li, C. P., "Numerical Solution of Viscous Reacting Blunt Body Flows of a Multicomponent Mixture," AIAA Paper 73-202, Washington, D.C., 1973.

[13] Bade, W. L. and Yos, J. M., "The NATA Code—Theory and Analysis," NASA CR-2547, June 1975.

[14] Hirschfelder, J. O., Curtiss, C. F., and Bird, R. B., *Molecular Theory of Gases and Liquids*, Wiley, New York, 1964, pp. 468-490.

[15] Cipolla, J. W., Jr., Lang, H., and Loyalka, S. K., "Temperature and Partial Pressure Jumps during Evaporation and Condensation of a Multicomponent Gas Mixture," in *Rarified Gas Dynamics*, edited by M. Becker and M. Fiebig; DFVLR-Press, Porz-Wahn, F.R. Germany, 1974.

[16] Curtiss, C.F. and Hirschfelder, J.O., *Journal of Chemical Physics*, Vol. 17, 1949, p. 550.

[17] Li, C. P., "Hypersonic Nonequilibrium Flow Past a Sphere at Low Reynolds Numbers," AIAA Paper 74-173, Washington, D.C., 1974.

[18] Svehla, R. A., "Thermodynamic and Transport Properties for the Hydrogen-Oxygen System," NASA SP-3011, 1964.

[19] McBride, B. J. and Gordon, S., "Fortran IV Program for Calculation of Thermodynamic Data," NASA TN D-4097, 1967.

[20] Vincenti, W. G. and Kruger, C. H., *Introduction to Physical Gas Dynamics*, Wiley, New York, 1965, p. 231.

[21] MacCormack, R. W., "Numerical Solution of the Interaction of a Shock Wave with a Laminar Boundary Layer," presented at the 2nd International Conference on Numerical Methods in Fluid Dynamics, Berkeley, Calif., 1970.

[22] Melin, G. A. and Madix, R. J., "Energy Accommodation During Oxygen Atom Recombination on Metal Surfaces," *Faraday Society Transactions*, Vol. 67, 1971, pp. 198-211.

[23] Rosner, D. E. and Feng, H. H., "Energy Transfer Effects of Excited Molecule Production by Surface-Catalyzed Atom Recombination," *Journal of Chemistry, Faraday Society Transactions Series*, Vol. 70, 1974, pp. 884-907.